C.P. No. 320
(18,335
A.R C Technical Report

C.P. No. 320
(18,335)
A.R C Technical Report

MINISTRY OF SUPPLY

AERONAUTICAL RESEARCH COUNCIL

CURRENT PAPERS

A Graphical Method of Predicting the Off Design Performance of a Compressor Stage

By

J. F. Louis and J. H Horlock

LONDON HER MAJESTY'S STATIONERY OFFICE

1957

PRICE 3s 6d NET

A Graphical Method of Predicting the Off Design Performance of a Compressor Stage

- By -

J. F. Louis and J. H. Horlock

April, 1956

1.0 Summary.- It has been seen in a previous paper (Ref. 1) that analytical solutions of compressor stage performance based on actuator disc theory are extremely difficult, and reliable only when the outlet angle distributions from the blade rows are the same at all flow rates. No analytical method is able to describe the flow when the stall is reached.

In order to overcome these difficulties a graphical method is developed for predicting stage off-design performance even when the stall occurs. The method is first used to predict the performance of a stage of "constant α_3" design, and experiments confirm the prediction. Next the method is used as a basis for comparison of different designs of a free-vortex stage.

2.0 Introduction.- In a compressor stage of three rows - guide vanes, rotor and stator, the flow through the guide vanes may be solved by assuming that the distribution of tangential vorticity with radius at exit from the row is unchanged by the presence of the nearby rotor (Ref. 1). The graphical method detailed here involves a determination of the static pressures at different radii which would satisfy the radial equilibrium condition far downstream of the following rotor row. This operation is repeated for different flow coefficients and the complete characteristics of the static pressure rise at different radii are obtained. The same method may be applied to determine the flow through the stator, and then to the next stages.

This method may be used in the "stalled" region as long as re-circulation does not appear at any section of the blades, and cascade data of sufficient accuracy are available.

The actuator disc theory of Ref. 2 is used in this paper.

2.1 Flow Through the Inlet Guide Vanes.- It has been found from experience of previous calculations that the interference effect between the guide vanes and the rotor may be neglected in determining c_{x_2} the velocity that would exist far down-stream of the guide vane row.

Using the nomenclature of Ref. 1 the equation describing the flow through the row is:

$$\frac{dc_{x_2}}{dr} = - \frac{2c_{x_{2e}} \tan \alpha_{2e}}{r\,(c_{x_2} + c_{x_1})} \frac{d}{dr} (rc_{x_{2e}} \tan \alpha_{2e}) \qquad \ldots(1)$$

Generally this equation may be solved analytically, and always numerically, without any special difficulty, by assuming that $c_{x_{2e}} = c_{x_2}$ or $c_{x_{2e}} = yc_{x_2}$ and $(1 - y)\, c_{x_1}$ where y is a constant, i.e., by neglecting the interference effect of the following rotor on the distribution of c_{x_2}. The solutions for c_{x_2} vary little with the different approximations.

2.2/

2.2 Flow Through the Rotor.- Using actuator disc theory, the flow is described by the equation:

$$\frac{dc_{x_3}}{dr} = -\frac{U}{rc_{x_{03}}}\frac{d}{dr}(rc_{x_{2e}}\tan\alpha_{2e}) + \frac{c_{x_3}}{rc_{x_{03}}}\tan\beta_{3e}\cdot\frac{d}{dr}[r(U - c_{x_{3e}}\tan\beta_{3e})] \qquad \ldots(2)$$

This equation is not linear, and can be linearized only for very simple variations with the radius of $\tan\alpha_{2e}$ and $\tan\beta_{3e}$, as has been seen previously (Ref. 1). No analytical solution is possible when the stall is reached. This form of the equation for the rotor is thus of no use in this case, where the complete off design performance is to be determined.

However, if the axial velocity far downstream of the rotor c_{x_3} is known, the flow is completely determined, and in particular at the leading and trailing edges of the blades, by the relations

$$\begin{aligned} c_{x_{2e}} &= \gamma c_{x_2} + \delta c_{x_3} + \mu c_{x_1} \\ c_{x_{3e}} &= \nu c_{x_3} + (1 - \nu)\, c_{x_2} \end{aligned} \qquad \ldots(3)$$

where γ, δ, μ, ν are constants.

The tangential velocities may then be calculated, and the static pressure distribution in the machine can also be determined. Far downstream of the rotor, the radial pressure distribution should balance the centrifugal acceleration.

Thus the ratio $\frac{c_{x_3}}{c_{x_1}}$ (which is to be determined) will be considered as a parameter for calculation the static pressure rise and the solution for c_{x_3} is obtained when there is radial equilibrium far downstream of the rotor. This calculation is made for the mean radii of three different annuli of equal area, into which the working area is divided, and may be repeated for various flow coefficients.

3.0 The Graphical Method (Fig. 1)

3.1 Steps in the Preparatory Calculation of the Pressure Rise Through Blade Sections (Fig. 1(a)).- A point on the pressure rise characteristic for a given radius may be determined for a selected flow coefficient. In this analysis the position of the centre of pressure (and the actuator disc) is assumed to be at midchord when the cascade is not stalled and at the leading edge when it is stalled. The steps in the calculation of the pressure rise characteristics (root, mean and tip) of Fig. 1a are: the determination of

(a) the distribution of c_{x_2} with radius using equation (1)

(b) a value of $c_{x_{2e}}$ using equation (3) and an assumed value of c_{x_3}

(c) the inlet angle to the rotor from the relation

$$\tan\beta_{2e} = \frac{U}{c_{x_{2e}}} - \tan\alpha_{2e}$$

(d)/

(d) the incidence on to the rotor at this flow coefficient.

(e) the outlet angle from the rotor row using Howell's data (Ref. 3)

(f) the loss coefficient from Howell's data and hence the actual losses in the rotor

(g) the pressure drop through the inlet guide vanes, applying Bernoulli's equation

(h) the pressure rise through the rotor applying Bernoulli's equation relative to the rotor and using the losses obtained from (f)

(i) the pressure variation from the trailing edge to far downstream, as the axial velocity changes from $c_{x_{2e}}$ to c_{x_2} the tangential velocity remaining constant

(j) algebraic addition of the pressure changes through guide vanes and rotor losses, giving the static pressure far downstream of the rotor.

Repeating this operation for different flow coefficients, complete characteristics of pressure rise against flow coefficient are determined for different radii and ratios of $\frac{c_{x_2}}{c_{x_1}}$, and the set of curves (Fig. 1a) can be drawn. Another graph relating $\tan \beta_{2e}$ to the flow coefficient $\frac{c_{x_1}}{U_m}$ can be drawn also (Fig. 1b) with $\frac{c_{x_2}}{c_{x_1}}$ as a parameter.

3.2 Graph Giving the Difference in Static Pressure Between Two Radii Far Downstream of the Rotor (Fig. 1d).- Figure (1c) gives the relative tangential velocity at the trailing edge of the rotor. The absolute tangential velocity is determined by the relation

$$\frac{c_{u_2}}{U_m} = \frac{c_{u_{2e}}}{U_m} = \frac{U}{U_m} - \frac{c_{x_{2e}}}{U_m} \tan \beta_{2e} \qquad \ldots(4)$$

The differential equation of the radial equilibrium condition is: $\frac{dp}{dr} = \rho \frac{c_u^2}{r}$ ...(5)

Using finite differences we may write (5): $\frac{\Delta p}{\Delta r} = \rho \frac{c_u^2}{r}$ and assuming that the variation of $\frac{c_u^2}{r}$ with the radius is linear, (5) becomes

$$\frac{dp}{\rho} = \tfrac{1}{2}\left(\frac{c_{u_a}^2}{r_a} + \frac{c_{u_b}^2}{r_b}\right)(r_b - r_a) \qquad \ldots(6)$$

if r_a and r_b are the two radii considered. Generally, three annuli will be considered and the radial equilibrium curves satisfying equation (5) can be drawn (Fig. 1d).

The/

The graph (1e) relates $\frac{c_{x_{3e}}}{c_{x_1}}$ to $\frac{c_{x_3}}{c_{x_1}}$ (using equation (4)); the line U must be considered when the row is unstalled and line S when it is stalled.

4.0 An Example of the Graphical Method.- The problem to be solved is to predict the off-design performance of a free-vortex stage of which the design point is

$$\left\{\begin{array}{l} \dfrac{K_p \Delta T}{U_m^2} = 0.22 \\[2ex] \dfrac{c_{x_1}}{U_m} = 0.65 \\[2ex] \tan \alpha_2 = \dfrac{0.154}{r} \\[2ex] \tan \beta_{3e} = -\dfrac{0.410}{r} + \dfrac{r}{0.4934} \end{array}\right.$$

and the figures 1 are related to this case. At the design point, the working points are given on Fig. 1a as $\frac{c_{x_1}}{U_m} = 0.65$ and $\frac{c_{x_3}}{c_{x_1}} = 1.0$ at the three different mean radii. The next working points to be determined are for a flow coefficient $\frac{c_{x_1}}{U_m} = 0.6$. It is first assumed that $\frac{c_{x_3}}{c_{x_1}} = 1$ at the different radii. Fig. 1b gives $\tan \beta_{3e}$ for the different radii. The absolute tangential velocities are:

at the root $\dfrac{c_{u_3}}{U_m} = 0.725 - \dfrac{c_{x_{3e}}}{U_m} \tan \beta_{3e} = 0.725 - 0.211 = 0.514$

at the mean $\dfrac{c_{u_3}}{U_m} = 1.0 - \dfrac{c_{x_{3e}}}{U_m} \tan \beta_{3e} = 1.0 - 0.593 = 0.407$

at the tip $\dfrac{c_{u_3}}{U_m} = 1.21 \dfrac{c_{x_{3e}}}{U_m} \tan \beta_{3e} = 1.21 - 0.941 = 0.369$

These values enable the determination of the points A, B, C on the graph (1d); AB gives the difference of pressure between root and mean and AC gives the difference of pressure between mean and tip. As it is known

that/

that the ratio at the mean is almost equal to 1.0 the distance AB is plotted from E (Fig. 1a) so that EF = AB, and in the same way EG = AC.

The positions of E, F, G give by interpolation the ratios:

$$\text{at the root} \quad \frac{c_{x3}}{c_{x1}} = 0.974$$

$$\text{at the mean} \quad \frac{c_{x3}}{c_{x1}} = 1.0$$

$$\text{at the tip} \quad \frac{c_{x3}}{c_{x1}} = 1.025$$

In general these ratios may not satisfy the continuity relation. In order to check this relation they may be corrected for a next approximation as follows:

		(from graph 1c)	
root	$\frac{c_{x3}}{c_{x1}} = 0.975$	$\frac{c_{x_{3e}}}{c_{x1}} = 0.981$	$\frac{c_{u_{3e}}}{U_m} = 0.516$
mean	$\frac{c_{x3}}{c_{x1}} = 1.000$	$\frac{c_{x_{3e}}}{c_{x1}} = 1.000$	$\frac{c_{u_{3e}}}{U_m} = 0.402$
tip	$\frac{c_{x3}}{c_{x1}} = 1.025$	$\frac{c_{x_{3e}}}{c_{x1}} = 1.020$	$\frac{c_{u_{3e}}}{U_m} = 0.354$

This second approximation introduces very slight changes in the static pressure distribution and the velocity profile used in the second approximation.

Repeating these graphical operations for decreasing $\frac{c_{x1}}{U_m}$ the operating points are determined usually after two or three approximations. Final characteristics are drawn in Fig. 1a and corresponding axial velocity profiles are plotted in Fig. 2. Operating points on Howell's curve of deflection against incidence are shown in Fig. 3.

An analysis of these final characteristics is interesting because the mechanism of the stage stall is shown and allows the following conclusions:

(a) the root will stall for a flow coefficient $\frac{c_{x1}}{U_m} = 0.435$

(b)/

(b) the mean and the tip will not stall, but the static pressure rise across these sections will drop due to the local increase in $\frac{c_{x_3}}{c_{x_1}}$.

(c) When the stage is unstalled, the static pressure characteristic at the mean for $\frac{c_{x_3}}{c_{x_1}} = 1.0$ gives a general picture of the flow.

(d) When the stall is reached at a certain section, there is a pressure drop at this radius which induces a corresponding drop at the other sections in order to satisfy the radial equilibrium and continuity relations.

(e) From consideration of Fig. 2 recirculation at the root may be expected for $0.4 > \frac{c_{x_1}}{U_m} > 0.375$.

5.0 Flow Through the Stator.- As the flow downstream the rotor has been solved, for each ratio $\frac{c_{x_3}}{c_{x_1}}$ the axial velocity can be calculated at the leading edges of the stator, as

$$c_{x_{4e}} = \alpha c_{x_2} + \beta c_{x_3} + \gamma c_x$$

$$c_{x_{4e}} = \delta c_{x_4} + \epsilon c_{x_3}$$

where $\alpha, \beta, \gamma, \delta, \epsilon$ are constant.

As the pressure distribution far downstream of the rotor and the axial velocity at the leading edge of the stator are known, the pressure distribution can be determined at the stator inlet. Similar steps in calculating the pressure rise through the blade section as in 3.1 are followed and the method is repeated in order to find the flow through the stator.

Once the flow through the whole stage is known, a second approximation may be carried out taking in account the interference effect between all the rows.

6.0 Comparison Between Predicted and Experimental Pressure Characteristics for the First Stage of the Compressor Test Rig at the University of Cambridge.- This graphical method was first applied to predict the off-design performance of the first stage (inlet guide vanes and rotor) of a compressor rig at the University of Cambridge (a "constant α_3" design). An earlier paper by Horlock (Ref. 4) has described the rig and the theoretical and experimental investigations carried out.

For this application the pressure characteristics were determined at the radii 0.5, 0.7 and 0.9 and are given in Fig. 4. Here again this analysis gives some insight into the mechanism by which the rotor row stalls:

(a)/

(a) The tip only will stall (with reference to Howell's data) for a flow-coefficient $\frac{c_{x1}}{U_m} = 0.48$, and when $\frac{c_{x1}}{U_m}$ is less than 0.45 there is a steep drop in static pressure at the tip section.

(b) The pressure characteristics for the mean and root radii do not cross the stall line. At those sections the row will not stall; this is the consequence of the drop of pressure and acceleration of the flow induced by the tip stall.

The experimental curves are plotted on the same Fig. 4 in dotted lines; at the design point $\left(\frac{c_{x1}}{U_r} = 0.67\right)$, the predicted static pressure coefficients are confirmed by experiment but with decreasing flows there is an increasing discrepancy between experimental surveys and the theory, principally at root and tip sections.

This is understandable, for in the prediction of the vortex flow two dimensional cascade data only were used and boundary layer effects, tip leakage and secondary flow effects were neglected.

At a flow coefficient $\frac{c_{x1}}{U_m} = 0.48$, the pressure drop predicted for $= 0.45$ occurs. In a previous experimental investigation on this first stage (Ref. 5) it was reported that stall propagation appears at the rotor tip section for $\frac{c_{x1}}{U_m} = 0.48$ and that only this area was stalled for decreasing flows. For $\frac{c_{x1}}{U_m} = 0.415$ the slopes of the experimental pressure characteristics become smooth, and this can probably be explained by a recirculation at the blade tip.

The difference between stall propagation in the compressor and stall in two dimensional cascades on which the prediction was based may explain the discrepancy in the pressure drop at the stall point.

The graphical method thus gives a clear indication of the mechanism of the stalling of a blade row.

7.0 Comparison of Free Vortex Stages.- Next the method was applied to study the off-design performances of different free-vortex stages designed for the same design conditions $\frac{k_p \Delta T}{U^2_m} = 0.22$ $\frac{c_{x1}}{U_m} = 0.65$ and the same distribution of solidity along the radius.

These stages differ by the amount of whirl given by the inlet guide vanes. The description of the air angles is:

for stage A_o $\quad \tan \alpha_{ae} = 0 \quad \tan \beta_{ae} = \frac{0.257}{r} + \frac{r}{0.493}$

for stage A_1 $\quad \tan \alpha_{ae} = \frac{0.154}{r} \quad \tan \beta_{ae} = -\frac{0.411}{r} + \frac{r}{0.493}$

for/

for stage A_2 $\quad \tan \alpha_{2e} = \dfrac{0.308}{r} \quad \tan \beta_{3e} = -\dfrac{0.565}{r} + \dfrac{r}{0.493}$

In the figures 1, 5 and 8 the graphs of the pressure rise coefficient are presented. It is predicted that the stages A_0 and A_1 will stall at the root and A_2 first at the mean.

On Howell's curves of deflection against incidence (Figs. 3, 7 and 10) are plotted the operating points at the different sections for decreasing flow coefficients. It can be seen that the rotor root reaches the stall first, principally because at the design point $\dfrac{c_{x1}}{U_m} = 0.65$, $\dfrac{i - i^*}{\epsilon^*}$ is smallest at the root section. This is because the lift coefficient, or the loading factor (defined by Carter) (Ref. 6) is maximum at the root section.

On Figs. 2, 6 and 9 the estimated velocity profiles are plotted. As the axial velocity is the smallest at the root (A_1 and A_0), the incidence will be increased and this will help to stall this section earlier.

For the stage A_2, $\tan \beta_{3e} < 0$ at the root, $\dfrac{dc_{x_{3e}}}{dr} < 0$ and this will delay the root stall. For the stage A_0, the method has been applied to a complete stage (rotor and stator). As the flow at the outlet from the stator is axial, the pressure characteristics are superimposed. The analysis shows that the stator root and mean sections stall together for a flow coefficient $\dfrac{c_{x1}}{U_m} = 0.475$. The stator stalls before the rotor. The pressure rise characteristics for the complete stage may be compared on Fig. 11 with the same characteristics at different radii downstream of the rotor. Fig. 12 shows the very steep velocity profiles predicted downstream of the stator, at off design conditions.

To conclude, this graphical method of analysis of the off-design performance may enable a choice of the best stage design to be made.

References

No.	Author(s)	Title, etc.
1	J. F. Louis and J. H. Horlock	Some aspects of compressor design. Current Paper No. 319. April, 1956.
2	J. H. Horlock	Some actuator disc theories for the flow of air through axial turbomachines. R. & M. 3030. December, 1952.
3	A. R. Howell	The present basis of axial compressors design. Part I. Cascade and theory performance. R. & M. 2095. June, 1942.
4	P. Ruden	Investigation of single stage axial flow fans. N.A.C.A. Tech. Memo. 1062. 1944.

5/

No.	Author(s)	Title, etc.
5	J. H. Horlock	Theoretical and experimental investigation of the flow through two single stage axial flow compressors. R. & M. 3031. March, 1955.
6	M. D. Wood J. H. Horlock and E. K. Armstrong	Experimental investigation of the stalled flow of a single stage compressor. A.R.C. 17,280. November, 1954.
7	A. D. S. Carter	The low speed performance of related aerofoils in cascades. Current Paper 29. September, 1949.

PREDICTED OFF DESIGN PERFORMANCES FOR THE STAGE A_1

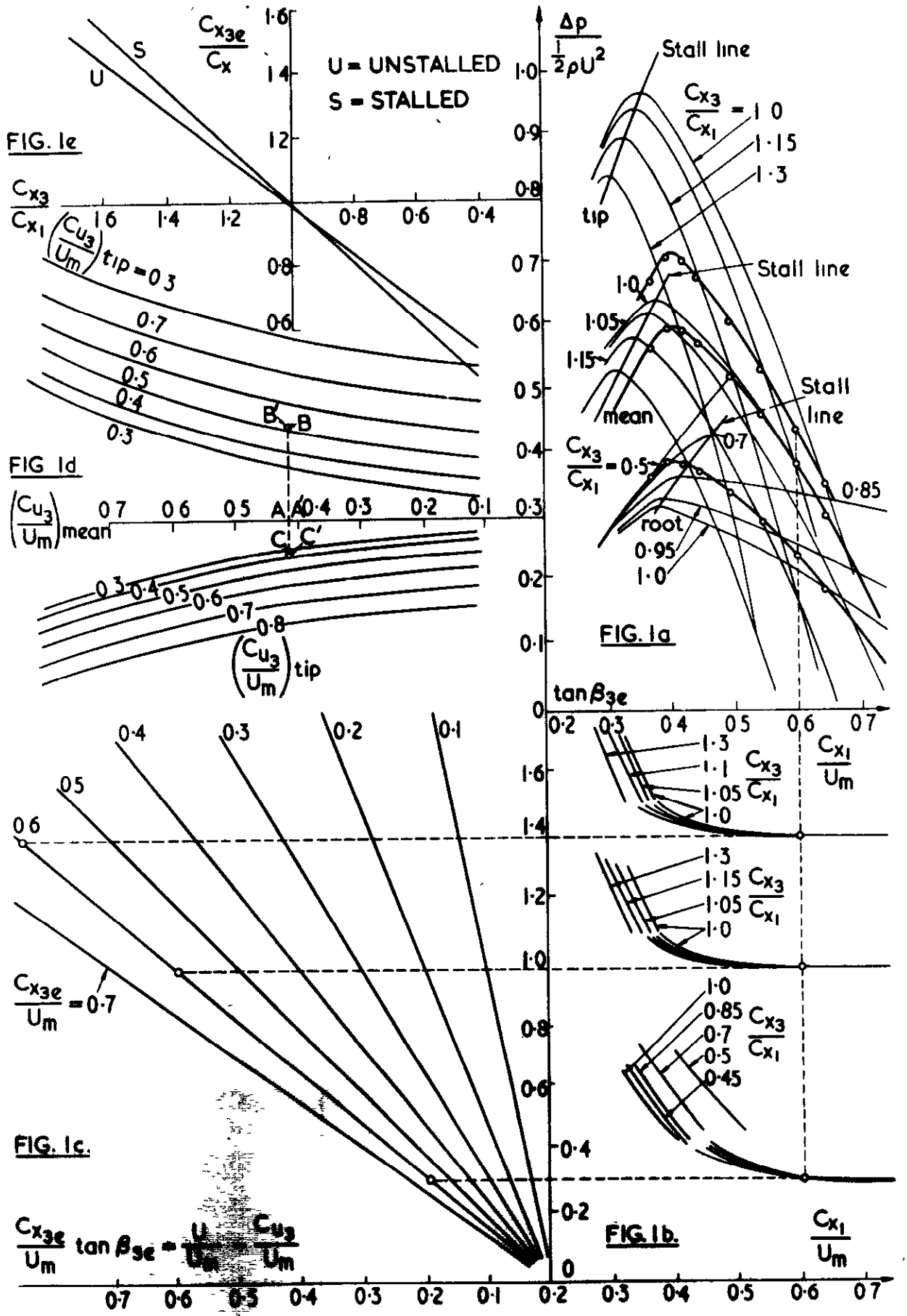

FIG. 2. PREDICTED VELOCITY PROFILES FOR DIFFERENT FLOW COEFFICIENTS IN THE FREE VORTEX STAGE A_1

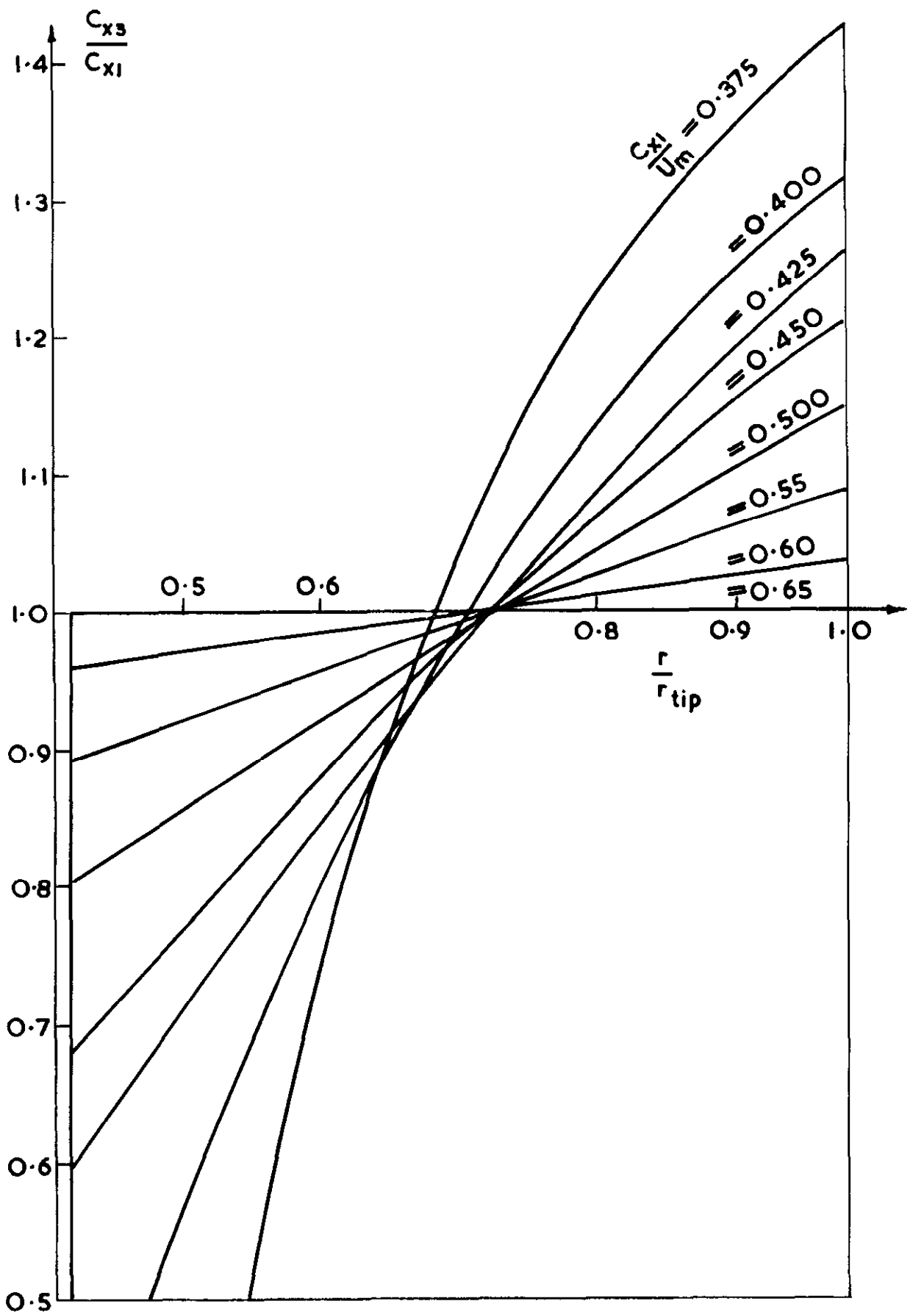

FIG. 3. OPERATING POINTS AT THE DIFFERENT RADII PLOTTED ON HOWELL'S CURVES.

(THE $\frac{i - i^*}{\epsilon^*}$ AXIS HAS BEEN SHIFTED FOR THE CURVES RELATED TO THE MEAN AND TIP RADII)

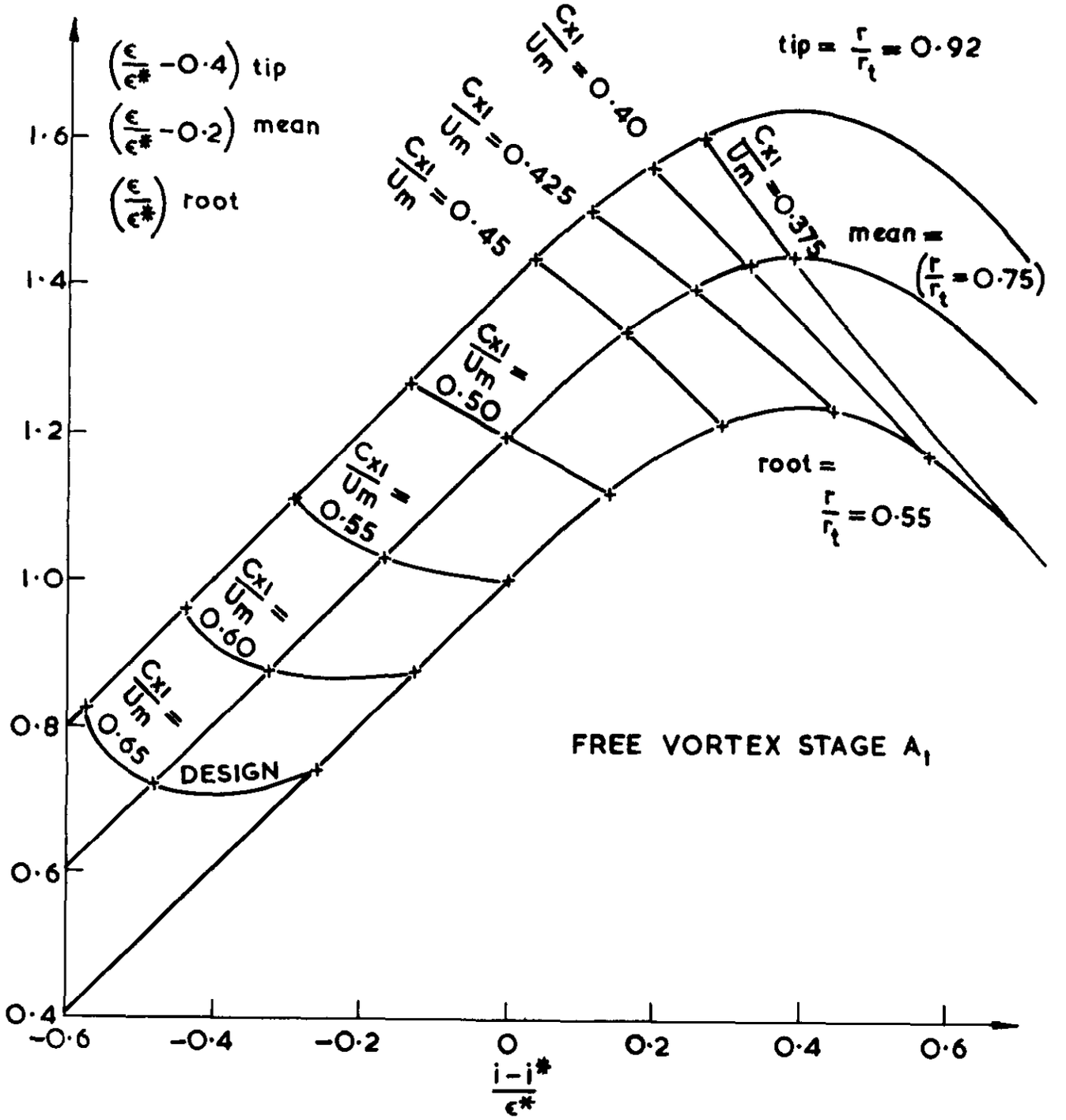

FIG. 4 PREDICTED AND EXPERIMENTAL PRESSURE CHARACTERISTICS AT DIFFERENT RADII MEASURED ON THE COMPRESSOR TEST RIG.

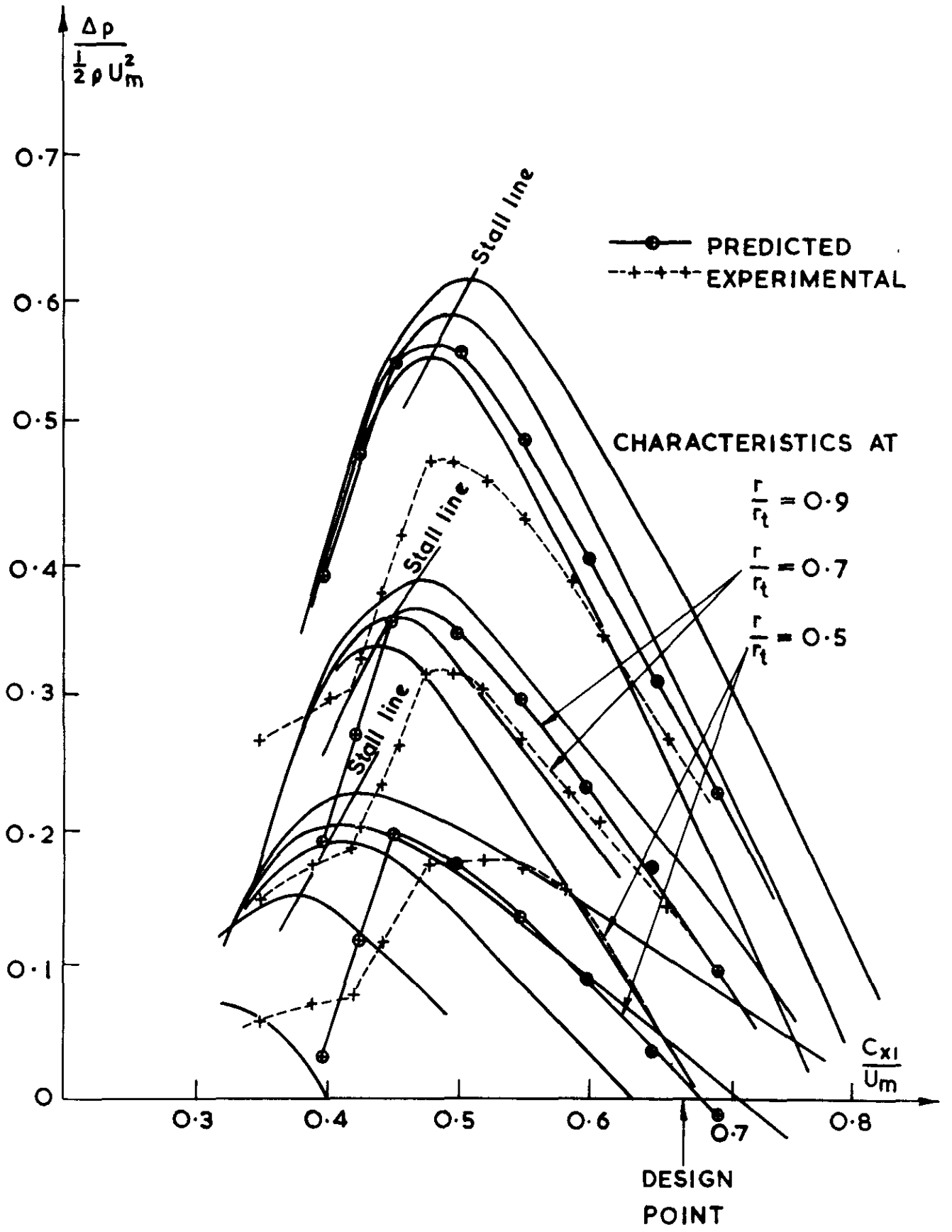

FIG. 5. PREDICTED PRESSURE CHARACTERISTICS AT DIFFERENT RADII FOR THE FREE VORTEX STAGE A_0

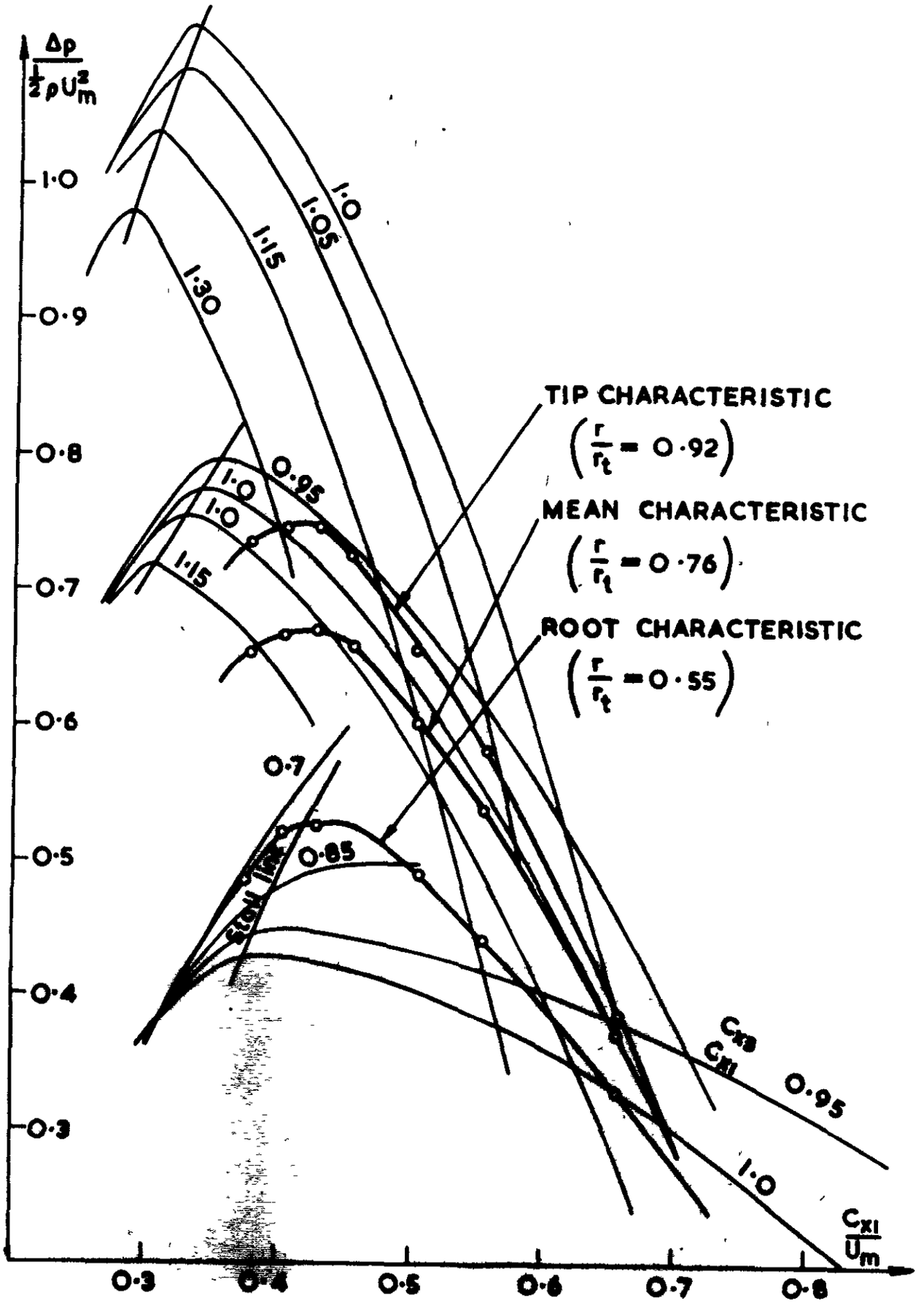

FIG. 6. PREDICTED VELOCITY PROFILES FOR DIFFERENT FLOW COEFFICIENTS IN THE FREE VORTEX STAGE A_0

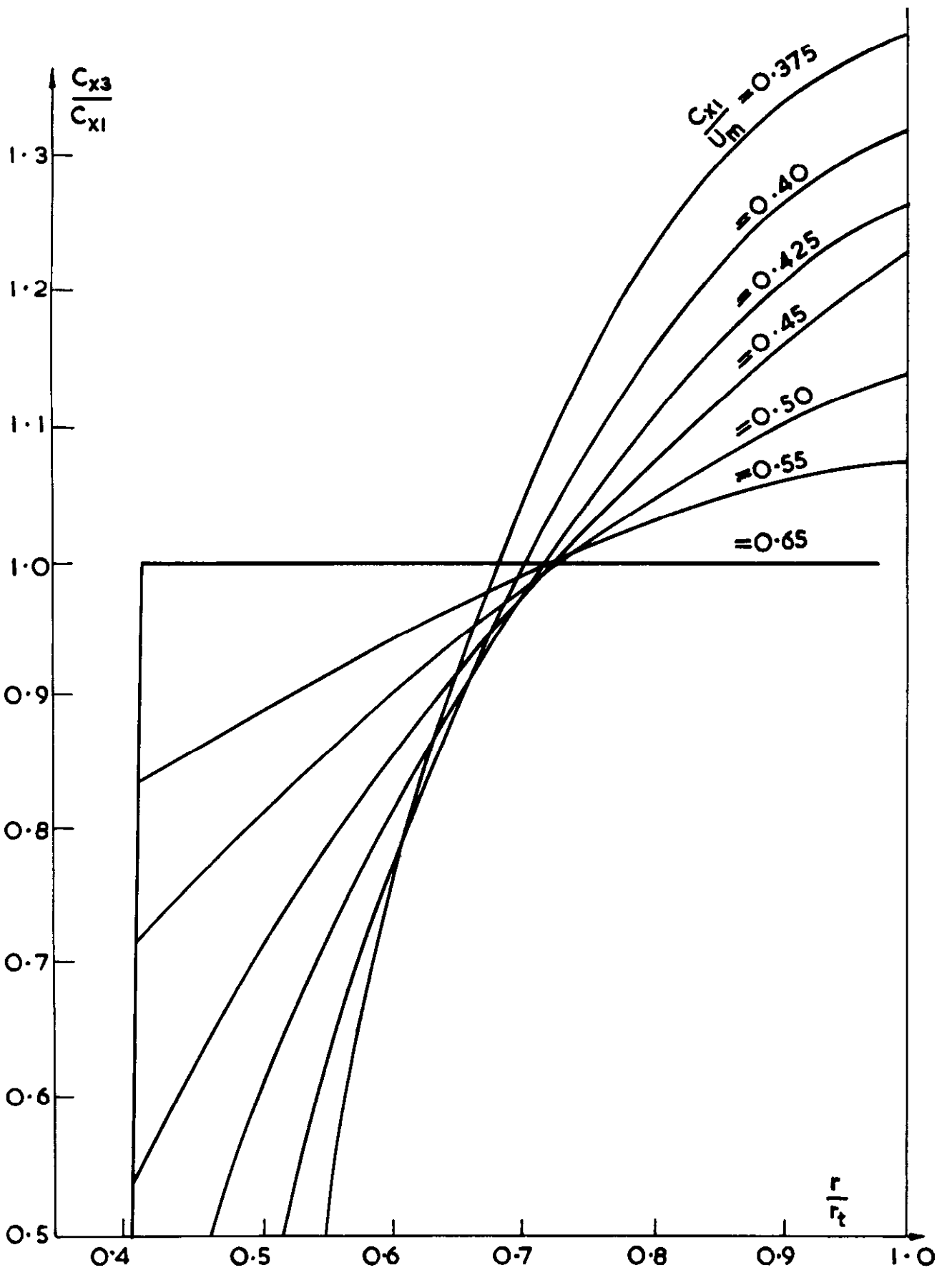

FIG. 7. OPERATING POINTS AT THE DIFFERENT RADII PLOTTED ON HOWELL'S CURVES

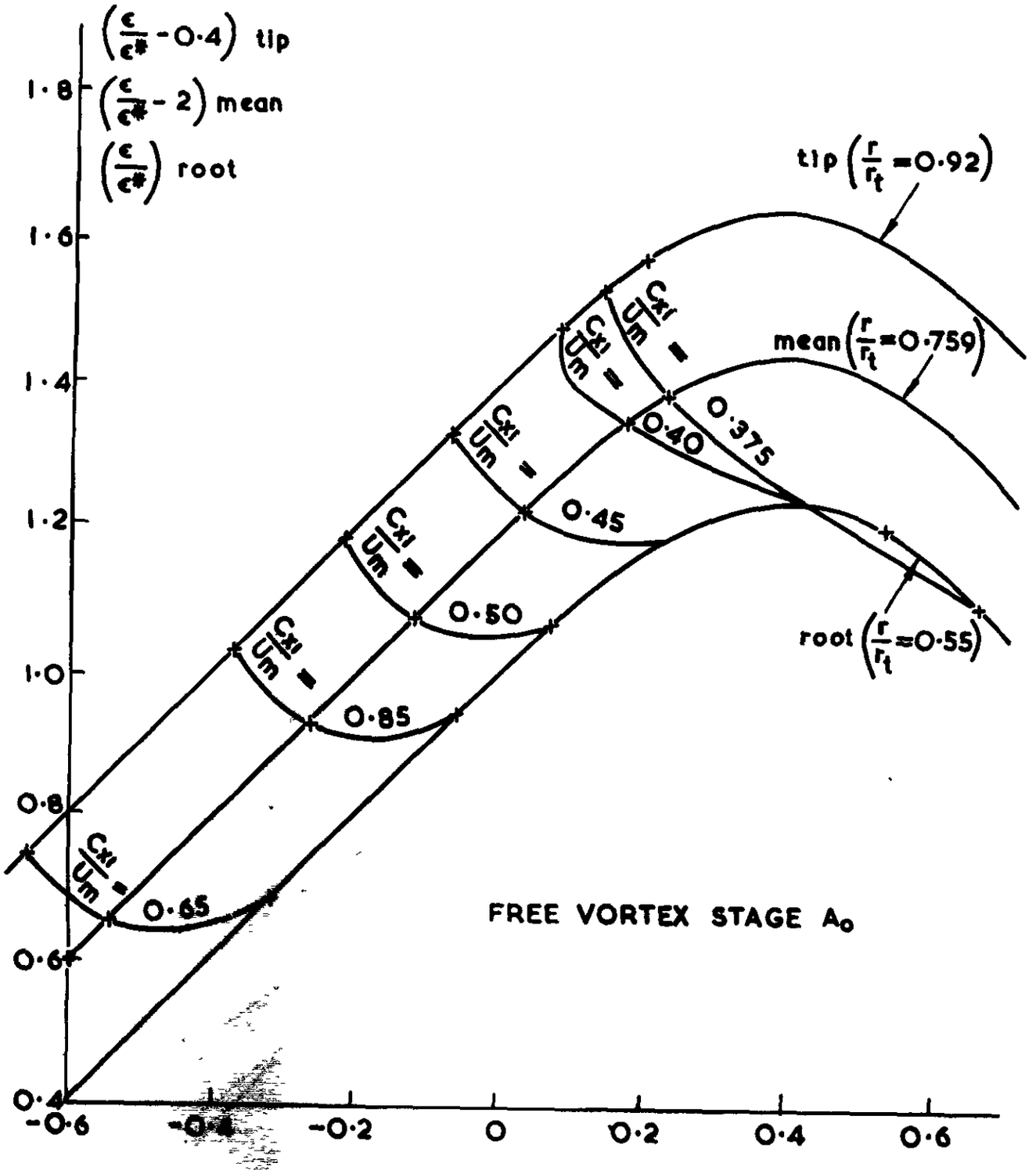

FIG 8. PREDICTED PRESSURE CHARACTERISTICS AT DIFFERENT RADII FOR THE FREE VORTEX STAGE A_2

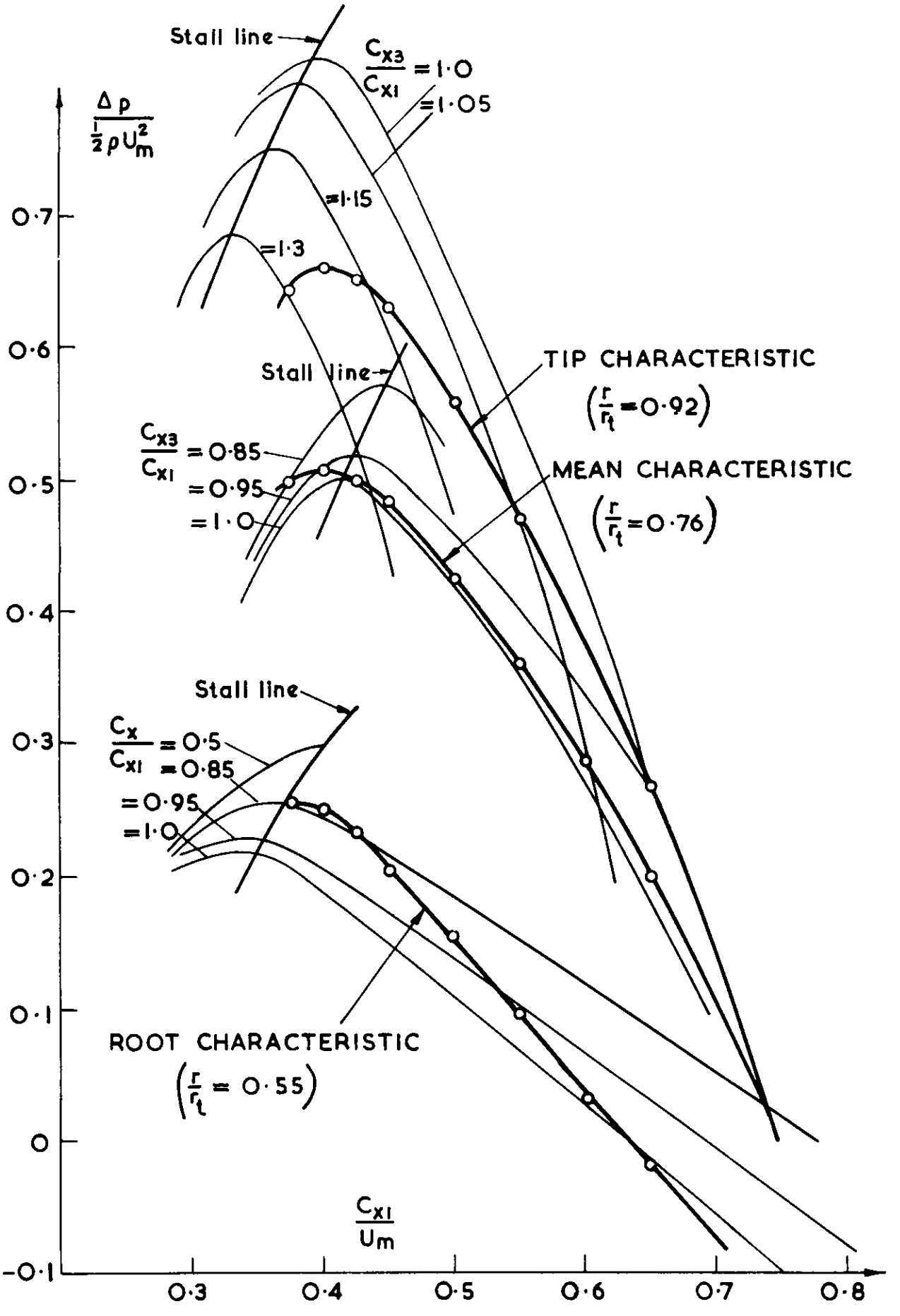

FIG. 9. PREDICTED VELOCITY PROFILES FOR DIFFERENT FLOW COEFFICIENTS IN THE FREE VORTEX STAGE A_2

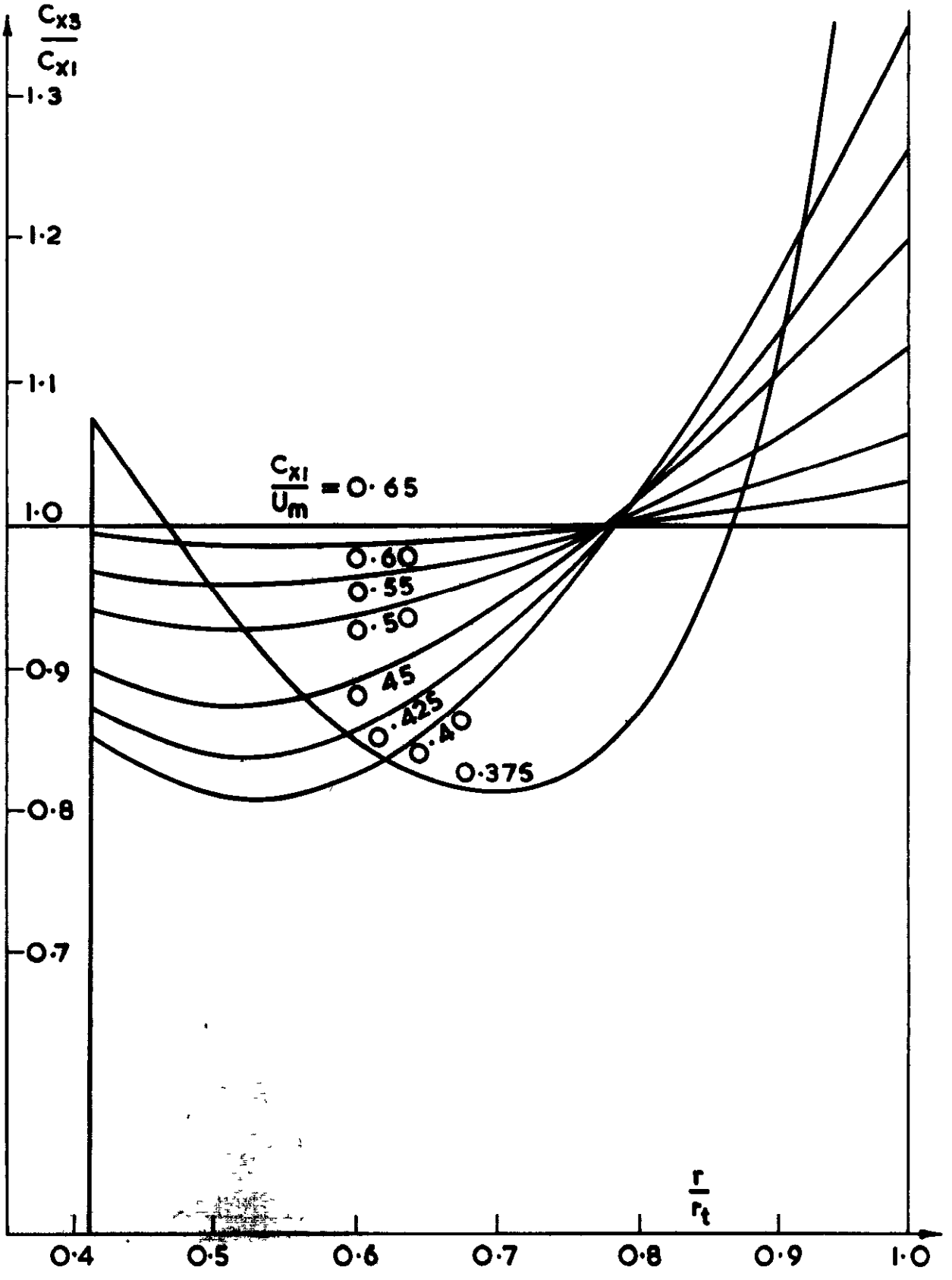

FIG. 10. OPERATING POINTS AT THE DIFFERENT RADII PLOTTED ON HOWELL'S CURVES

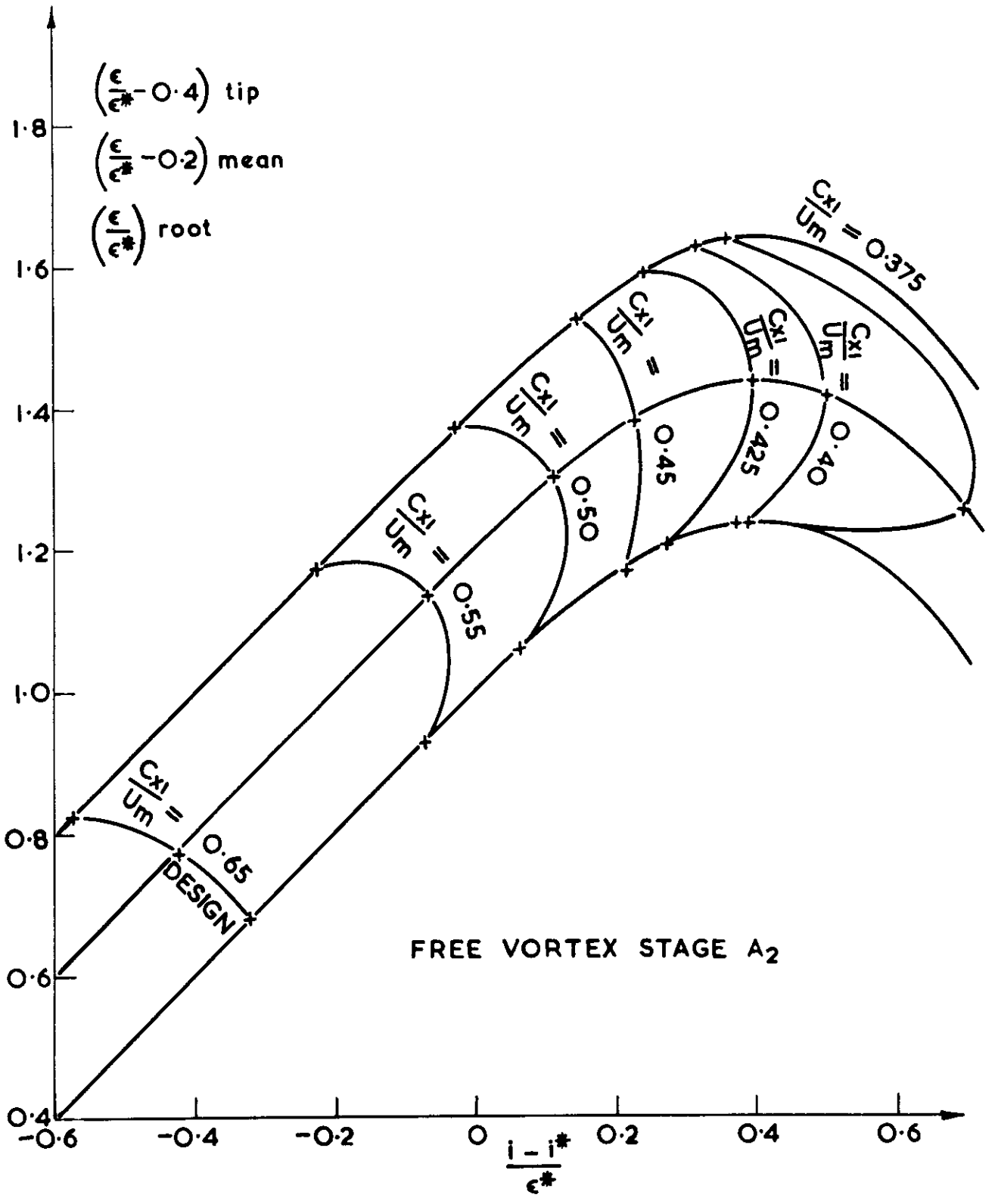

FIG. 11. PREDICTED PRESSURE CHARACTERISTICS AT DIFFERENT RADII FOR THE COMPLETE FREE VORTEX STAGE A_0 ROTOR AND STATOR

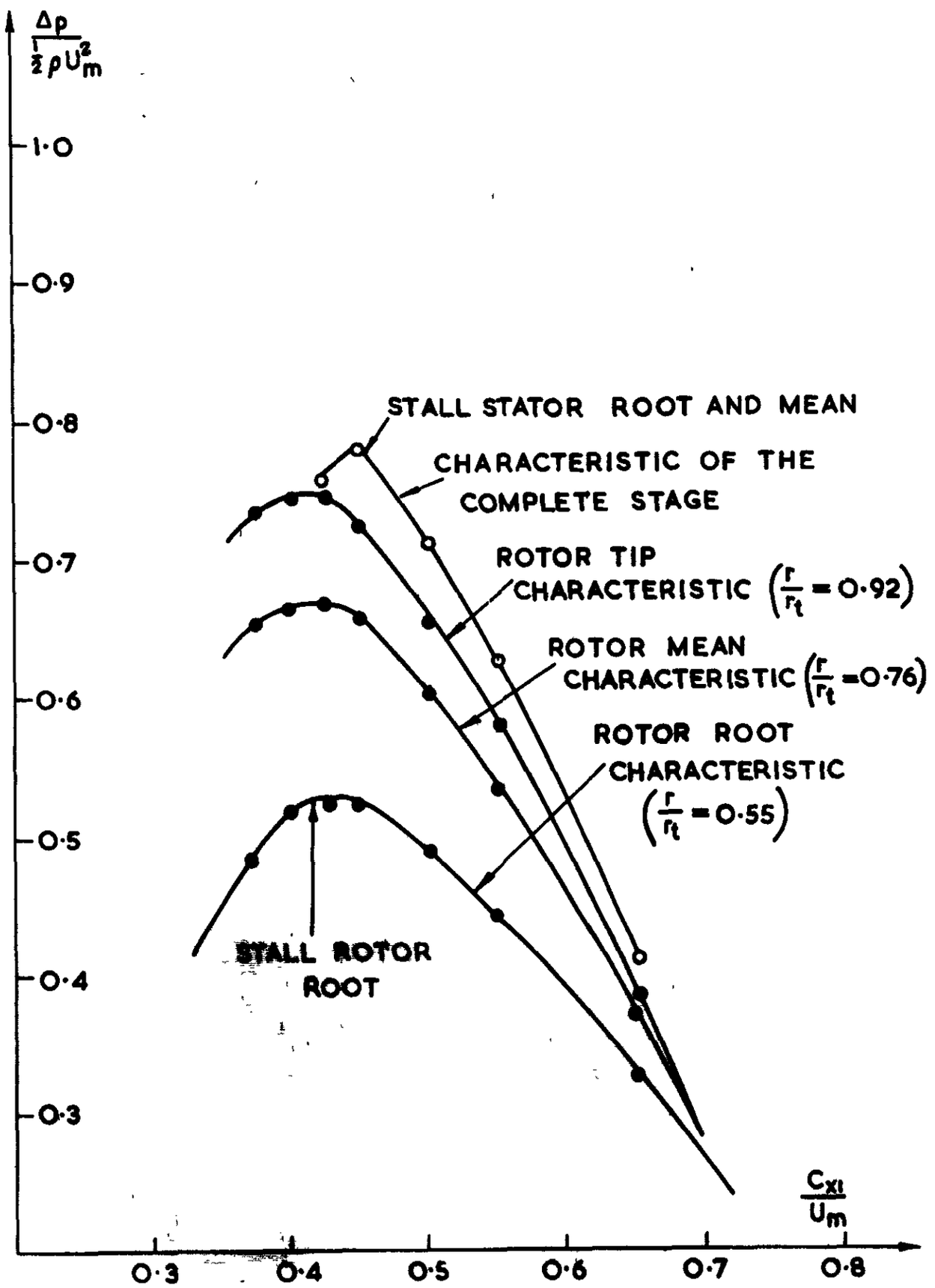

STAGE A_o

FIG. 12. PREDICTED VELOCITY PROFILES AT STATOR OUTLET FOR DIFFERENT FLOW COEFFICIENTS

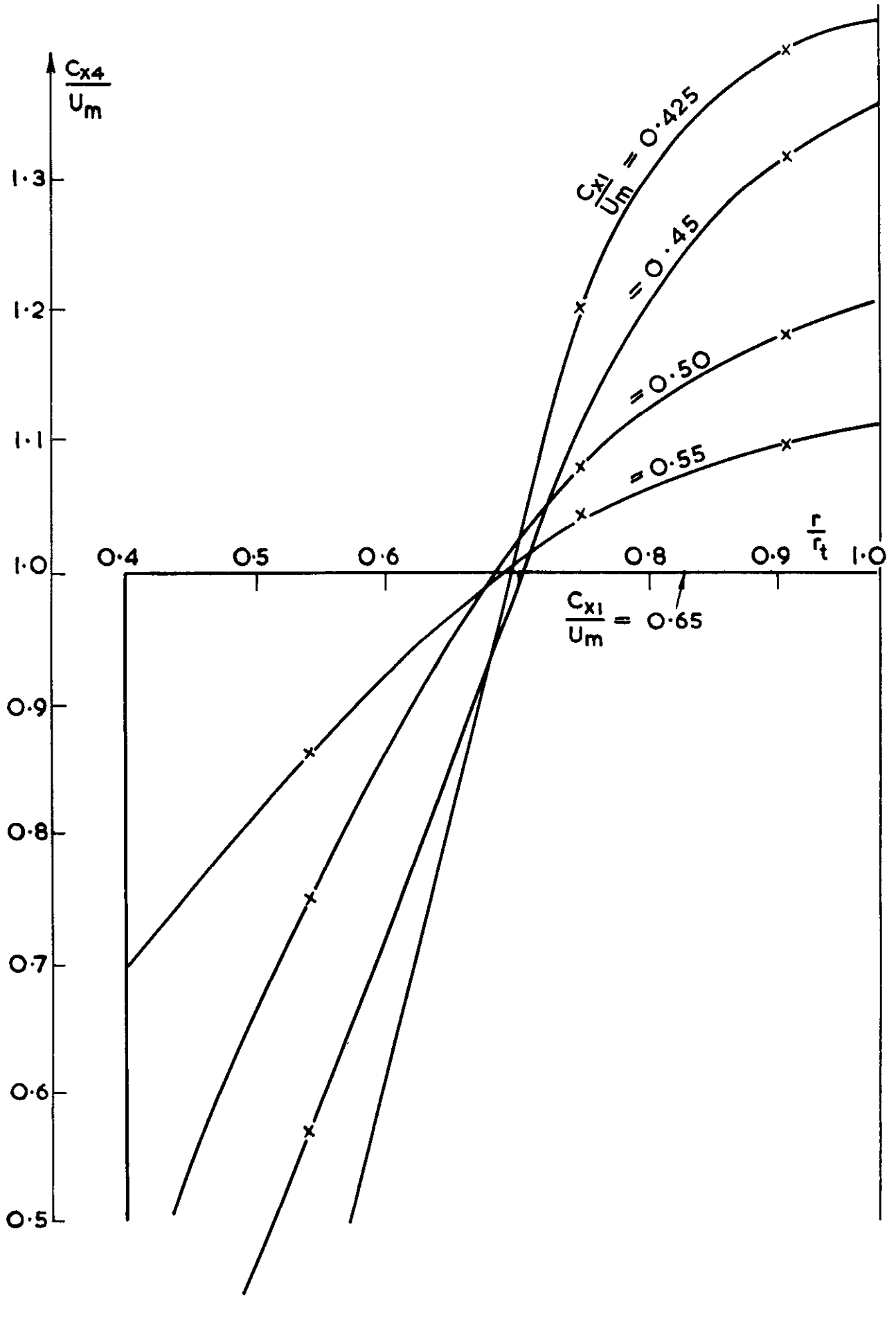

C.P. No. 320
(18,335)
A.R.C. Technical Report

Printed and published by
HER MAJESTY'S STATIONERY OFFICE

To be purchased from
York House, Kingsway, London W.C.2
423 Oxford Street, London W.1
P.O. Box 569, London S.E.1
13A Castle Street, Edinburgh 2
109 St. Mary Street, Cardiff
39 King Street, Manchester 2
Tower Lane, Bristol 1
2 Edmund Street, Birmingham 3
80 Chichester Street, Belfast
or through any bookseller

Printed in Great Britain

S.O. Code No. 23-9010-20

C.P. No. 320